A barium titanate-on-oxide insulator optoelectronics platform

Yu Cao, Siew Li Tan, Eric Jun Hao Cheung, Shawn Yohanes Siew, Changjian Li, Yan Liu, Chi Sin Tang, Manohar Lal, Guanyu Chen, Karim Dogheche, et al.

A Barium Titanate-on-Oxide Insulator Optoelectronics Platform

Yu Cao, Siew Li Tan, Eric Jun Hao Cheung, Shawn Yohanes Siew, Changjian Li, Yan Liu, Chi Sin Tang, Manohar Lal, Guanyu Chen, Karim Dogheche, Ping Yang, Steven Pennycook, Andrew Thye Shen Wee, Soojin Chua, Elhadj Dogheche, Thirumalai Venkatesan, and Aaron Danner**

Electro-optic modulators are among the most important building blocks in optical communication networks. Lithium niobate, for example, has traditionally been widely used to fabricate high-speed optical modulators due to its large Pockels effect. Another material, barium titanate, nominally has a 50 times stronger *r*-parameter and would ordinarily be a more attractive material choice for such modulators or other applications. In practice, barium titanate thin films for optical waveguide devices are usually grown on magnesium oxide due to its low refractive index, allowing vertical mode confinement. However, the crystal quality is normally degraded. Here, a group of scandate-based substrates with small lattice mismatch and low refractive index compared to that of barium titanate is identified, thus concurrently satisfying high crystal quality and vertical optical mode confinement. This work provides a platform for nonlinear on-chip optoelectronics and can be promising for waveguide-based optical devices such as Mach–Zehnder modulators, wavelength division multiplexing, and quantum optics-on-chip.

1. Introduction

Electro-optic modulators form an integral part of the telecommunications ecosystem, encoding binary information for transmission along fiber optic cables. Modulator speed greatly influences Internet data rates, and such modulation is achieved in fabricated optoelectronic devices using materials with an electro-optic effect, or Pockels effect. Among these materials, bulk lithium niobate is widely used in commercial modulators, and recent development in its thin-film form (lithium niobate-on-insulator) has attracted considerable attention, because its excellent optical mode confinement enables a high level of integration of photonic devices. An alternative material, barium titanate, has an electro-optic effect which is in principle 50 times stronger than that of lithium niobate. However, it is challenging to fabricate devices in barium titanate compared to lithium niobate, because a phase transition at 120 °C causes cracks in bulk barium titanate, and attempts at creating thin-film barium titanate-on-insulator with substrates such as magnesium oxide typically end up with degraded crystal quality. Here, we introduce a barium titanate-on-oxide insulator platform with a family of alternative low-index substrates that concurrently allow both high crystal quality and excellent vertical mode confinement. The grown single-crystal barium titanate thin film with a well-aligned *c*-axis orientation is ideal for electrode placement due to crystal symmetry considerations. Furthermore, we fabricated waveguides on barium titanate-on-dysprosium scandate as example devices and verified low optical propagation loss. The structure is stable at higher temperatures and does not suffer from the 120 °C phase

Dr. Y. Cao, Dr. S. L. Tan, E. J. H. Cheung, Dr. S. Y. Siew, Dr. Y. Liu, Dr. M. Lal, Dr. G. Chen, Prof. S. Chua, Prof. T. Venkatesan, Prof. A. Danner
Department of Electrical and Computer Engineering
National University of Singapore
4 Engineering Drive 3, Singapore 117583, Singapore
E-mail: venky@ou.edu; adanner@nus.edu.sg

Dr. Y. Cao, Prof. A. T. S. Wee, Prof. T. Venkatesan
Department of Physics
National University of Singapore
2 Science Drive 3, Singapore 117551, Singapore

Dr. C. Li, Dr. P. Yang, Prof. S. Pennycook
Department of Materials Science and Engineering
National University of Singapore
9 Engineering Drive 1, Singapore 117575, Singapore

Dr. C. S. Tang
NUS Graduate School for Integrative Sciences and Engineering
National University of Singapore
University Hall, Tan Chin Tuan Wing, Singapore 119077, Singapore

Dr. C. S. Tang, Dr. P. Yang
Singapore Synchrotron Light Source (SSLS)
National University of Singapore
5 Research Link, Singapore 117603, Singapore

Dr. K. Dogheche, Prof. E. Dogheche
Institute of Electronics, Microelectronics, and Nanotechnology, IEMN DOAE
Université Polytechnique Hauts-de-France
Valenciennes 59309, France

transition; this makes barium titanate-on-insulator an attractive option for future optoelectronics applications.

Single-crystal barium titanate (BTO, or $BaTiO_3$) has excellent textbook electro-optic properties, making it an attractive material for potential fabrication of nonlinear optical devices ($r_{51} = r_{42} = 1640$ pm V^{-1} in BTO vs $r_{33} = 30$ pm V^{-1} in lithium niobate).[1,2] Bulk BTO single crystals are expensive, and are difficult to process in such a way as to achieve good index contrast. However, a BTO thin film hypothetically grown on a substrate with a lower refractive index can be etched into single mode waveguides with good optical mode confinement within the BTO layer. BTO films ($n_o = 2.254$, $n_e = 2.178$) grown on magnesium oxide (MgO), which has a refractive index of 1.7,[3] have previously been used as a platform for fabricating electro-optic modulators.[4–11] However, due to the large lattice mismatch between MgO and BTO and the hygroscopic nature of MgO resulting in a poor surface, the crystal quality of BTO grown on MgO is normally degraded, and BTO thin films end up polycrystalline,[12,13] multi-domain,[7,14] or single crystal but with poor crystal quality.[9,11]

The electro-optic effect in polycrystalline barium titanate grown on MgO is already equivalent to that in single-crystal lithium niobate,[12,13,15] and the *r*-parameter in poor single crystal or multi-domain barium titanate films can be several times larger.[7,11,14] Thus one would expect that with improved crystal quality of grown single-crystal BTO thin films the electro-optic effect would be further enhanced. The observed reduction of the *r*-parameter in BTO films on MgO compared to the bulk value can be partly attributed to mis-orientation of domains, which causes averaging out of the strong r_{42} and r_{51} matrix elements with much weaker *r*-values along incorrect crystal or field orientations, which cannot be avoided in multi-domain BTO. Aside from MgO, strontium titanate (STO, or $SrTiO_3$) has previously shown to be a superb substrate for high-quality single-crystal BTO growth, but its refractive index is unfortunately larger than that of BTO, making it unsuitable for creating optical slabs. An appropriate substrate choice needs to concurrently ensure both good crystal quality and optical confinement. Dysprosium scandate (DSO, or $DyScO_3$) has both of these qualities—a small lattice mismatch (≈1%) and a lower refractive index, making it a perfect substrate for BTO-thin-film-based optical devices. Here, we use dysprosium scandate to grow high quality single-crystalline *c*-axis aligned BTO films. We characterize the films by X-ray diffractometry (XRD) over a wide range of temperatures showing no phase transition up to 700 °C. We then fabricate single-mode waveguides and verify low loss. In this letter we also introduce other substrate candidates aside from DSO which can potentially support this barium titanate platform and we verify their optical properties.

2. Results and Discussion

First, growth quality of a typical 850 nm-thick BTO film grown on a 25 mm^2 substrate by pulsed laser deposition (PLD) is presented in **Figure 1**, illustrating a smooth surface and high single crystallinity. Figure 1a shows a smooth surface of the BTO thin film that has root-mean-square (RMS) roughness of 0.754 nm, and this smooth surface helps reduce light scattering in the resultant waveguides. Figure 1b shows the BTO films only have (001) and (002) peaks, indicating that the film has a single (001)/*c*-axis orientation, and the rocking curve measured at the BTO (002) peak has a full-width at half-maximum (FWHM) of 0.075 (Figure 1c), indicating the *c*-axes are very well aligned. High crystal quality is illustrated by the scanning transmission electron microscopy (STEM) image in Figure 1d. The atomically sharp interface between BTO and DSO also reduces the light scattering in the resultant waveguides. For waveguide applications, BTO a few hundred nanometers thick is required to achieve mode confinement, and thus the BTO films at such thickness are relaxed from their fully strained state (Figure 1e,f).

The ordinary and extraordinary refractive indices (respectively n_o and n_e) of BTO film on DSO are measured with the prism coupling method as a function of wavelength,[16] as shown in **Figure 2**a, and subsequently fitted with the Sellmeier equation. n_o follows the dispersion trend nicely; at one wavelength (984 nm) n_e has a discrepancy and is not included. The discrepancy results from the fact that the TM polarization is more difficult to couple into the slab waveguide than the TE polarization as an inherent result of the Fresnel Law, and missing modes can result in an incorrect estimate of the index. The trends are otherwise likely highly accurate.

It is worth noting that for DSO (110), the in-plane lattice constants are not equal ($a \neq b$), thus the lattice of grown BTO films seems to follow the substrate at an early growth stage, causing in-plane anisotropy. As BTO films thicken, relaxation is expected to reduce this difference. In any case, refractive indices for both directions were measured at 637 nm wavelength and only a small difference of 0.009 was noted.

Bulk BTO has a Curie temperature (T_C) of 125 °C which would ordinarily present potential process challenges,[17] but luckily the T_C in thin films is typically higher due to strain induced by the substrate. For a fully strained (50 nm) BTO-on-DSO film, the T_C is known from the literature to increase to 680 °C,[18] but such a thin BTO layer would be unsuitable for optoelectronics purposes. An appropriate thickness would be a few hundred nanometers, where the strain on the film is relaxed, with the T_C expected to be possibly lower than that of a fully strained BTO but higher than in the bulk. Figure 2b presents refractive indices at elevated temperatures for an 850 nm-thick BTO film on DSO. Both n_o and n_e increase linearly and do not coincide up to 200 °C, indicating that the T_C is at least higher than 200 °C. Note that the birefringence is almost unchanged as the temperature increases, maintaining a stable optical property. The temperature range of index measurement is limited by the instrument.

A hypothetically low phase-transition temperature of 125 °C would normally create difficulties during fabrication, because the structural phase transition which occurs due to heating (during etching, for example) can easily cause BTO to crack. However, BTO in the thin-film form is much more stable due to the increased T_C as atoms in the film are held firmly in place by strain mediation from the substrate (i.e., substrate clamping). We measured the lattice constants of a 500 nm-thick BTO film on DSO as a function of temperature (during heating and cooling). The results (**Figure 3**) show that the smooth change of lattice constants during cooling and heating up to

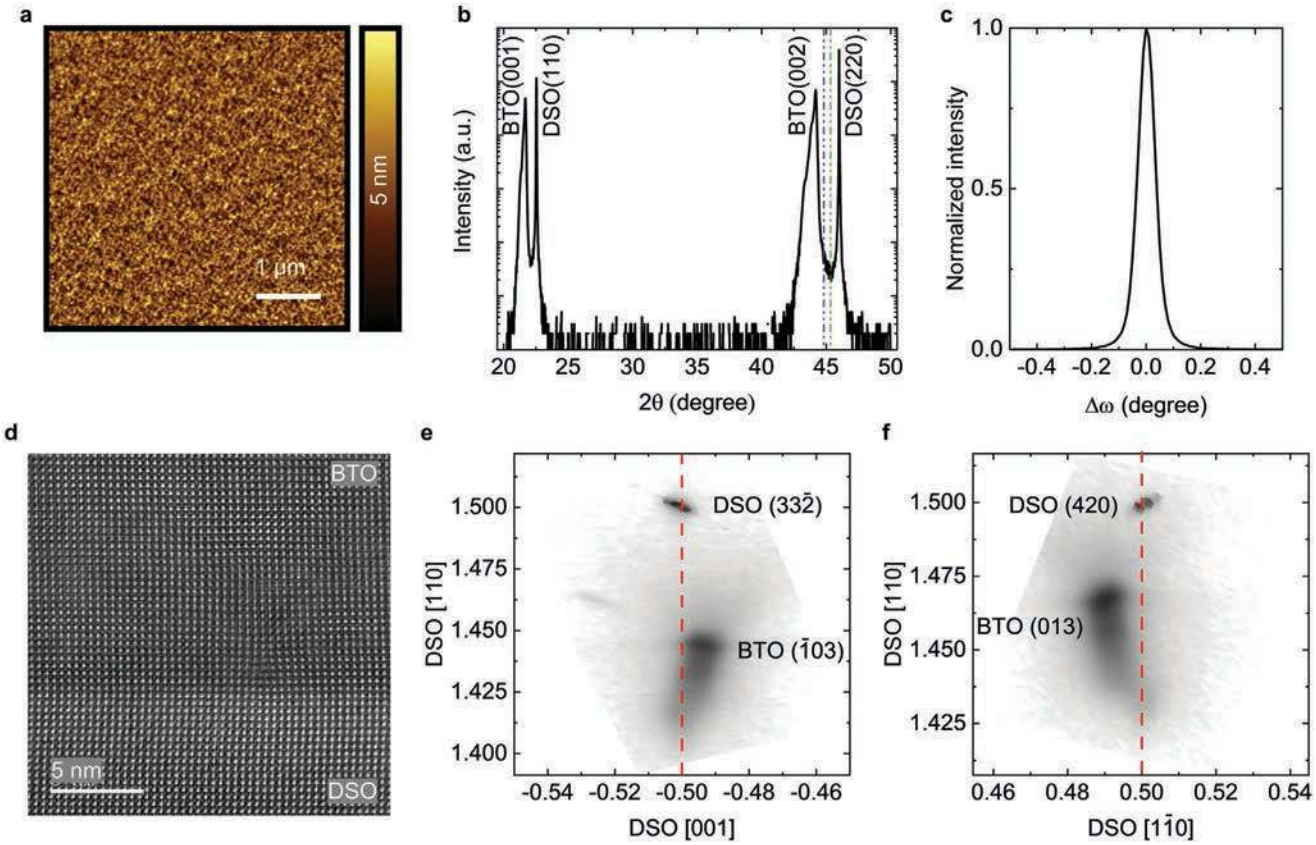

Figure 1. Crystal quality of 850 nm BTO film on DSO. a) AFM morphology image showing small roughness at the BTO surface of BTO on DSO, with RMS roughness of 0.754 nm. b) XRD 2θ–ω coupled scan showing that the BTO film is purely *c*-axis single crystal. The dash–dot lines in blue and green label the Bragg angles for the *c* plane and the *a* plane in bulk material, respectively. c) A small FWHM of 0.075° in the rocking curve of the BTO (002) Bragg peak verifies the high crystal quality of the BTO film. d) High-resolution STEM cross-sectional image of BTO on DSO showing the high crystal quality and the BTO's *c*-axis being orthogonal to the interface. e,f) XRD reciprocal space mapping (RSM) of BTO (–103) and (013) plane showing the relaxed nature of the BTO film. The red dashed lines label the fully strained lattice constant, indicating that the BTO film is relaxed at its thickness.

a temperature of 700 °C indicate no clear phase transitions or cracking, thus permitting all ordinary lithography, etching, and other fabrication processes to be executed.

We then fabricated waveguides for evaluation of optical propagation loss. Loss in the straight waveguides is characterized by the Fabry–Perot method.[19] For the Fabry–Perot

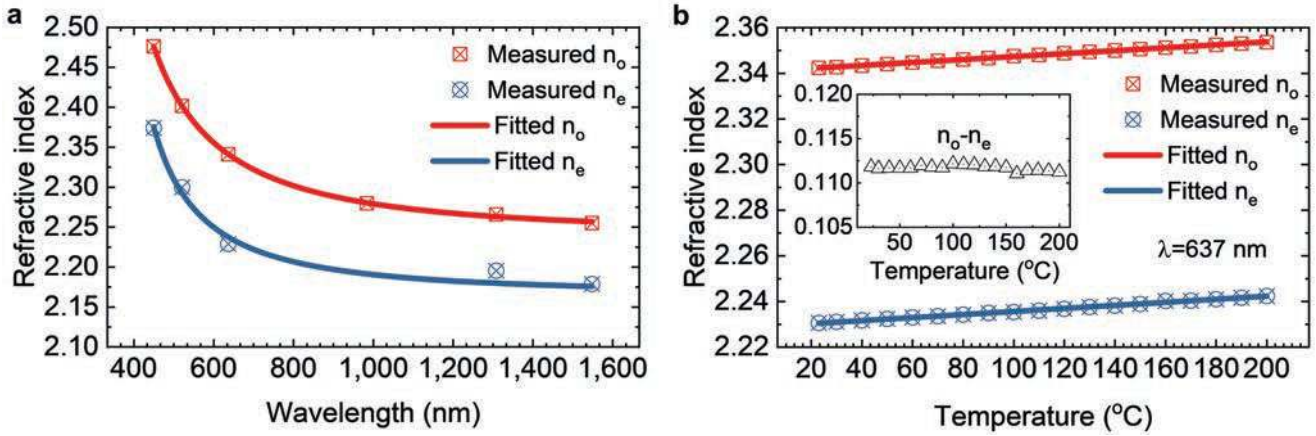

Figure 2. Optical properties of 850 nm-thick BTO-on-DSO. a) Refractive indices of BTO film as function of wavelength. n_o, n_e are measured at 450, 521, 637, 984, 1308, 1548 nm and fitted with the Sellmeier equation. The measurements are performed at room temperature. b) Measured (n_o, n_e) as a function of temperature are linearly fitted indicating phase stability of BTO films up to 200 °C. The difference between n_o and n_e plotted in the inset indicates a stable birefringence property.

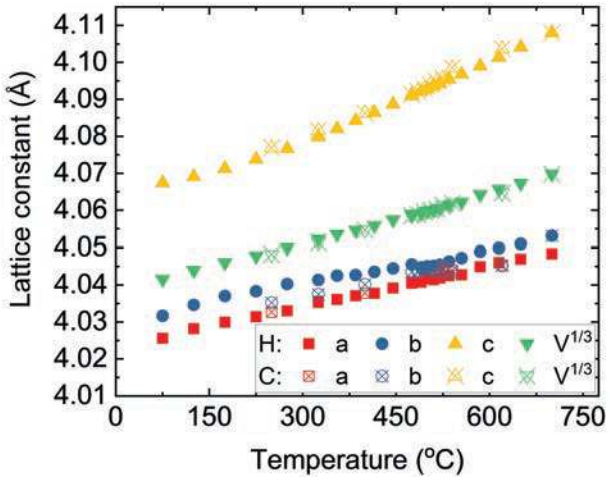

Figure 3. Lattice constant of BTO on DSO as a function of temperature. Lattice constants *a*, *b*, *c*, and unit cell volume *V* (normalized to $V^{1/3}$) of 500 nm-thick BTO-on-DSO as a function of temperature measured by XRD RSM during heating (solid symbols) and cooling (hollow symbols).

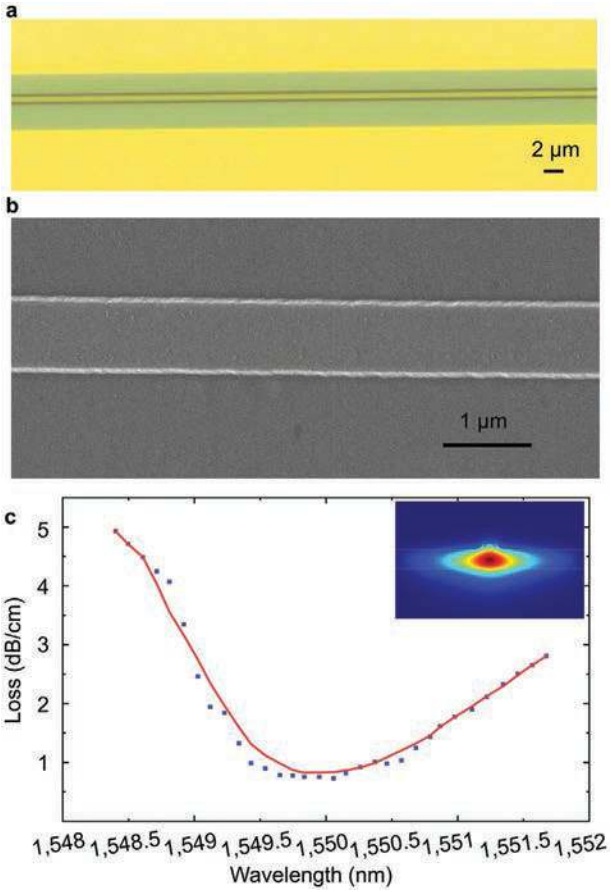

Figure 4. Propagation loss of BTO waveguide. a) Optical microscopy and b) helium-ion microscopy image of 0.7 μm-wide BTO ridge waveguide. c) Propagation loss characterized by the Fabry–Perot method. The inset shows the cross-sectional TE mode simulated by COMSOL.

method measurement (Figure S1, Supporting Information), a 0.7 μm-wide straight ridge waveguide is fabricated (800 nm BTO thin film with 170 nm etch depth), and **Figure 4**a,b shows the smooth surface and side wall of the etched waveguide. The transmission spectrum is subsequently measured and a low loss of about 2 dB cm^{-1} is obtained at wavelengths near 1550 nm (Figure 4c). We also measured the loss of this waveguide by the camera method which shows commensurate results (Figure S2, Supporting Information). The measured propagation loss in the BTO waveguides is comparable to that in ultralow-loss lithium niobate-on-insulator waveguides.[15,20–24]

Recently, a significantly large *r*-value of 923 ± 215 pm V^{-1} was achieved in multi-domain structured BTO grown on buffered silicon.[25] As in lithium niobate, a specific electrode orientation is needed in *a*–*c* domain BTO, bringing limitations for certain applications. In contrast, for our *c*-axis oriented BTO film, r_{51} and r_{42} are both in-plane and expected to be equal, therefore bringing the convenience of positioning co-planar electrodes along waveguides in any direction, potentially following curves, ring resonators, etc., while still achieving the maximum electro-optic effect.

The reported *a*-axis/or *a*–*c* domain in ref. [25] has a thin layer of BTO at the bottom with a high index strip loaded on top. In such a configuration, most of the power of the optical field is confined in the Si or SiN_x in such way that only a small fraction of the optical field overlaps the BTO and the modulation of refractive index in such a region is effectively performing a modulation of the whole device. In our BTO thin film, with a larger thickness of over 500 nm, the etched waveguide presented in the inset of Figure 4c has 92.0% of the optical field power distributed in the BTO crystal. Even though a satisfactory modulation effect has been achieved in Reference 25, there are still possible improvements. First, *a*-axis BTO thin film has *a*–*c* domain formation in-plane, where the *c*-axis is distributed in-plane with an angle to the desired field direction. Second, the effective planar electro-optic effect is not uniform in different directions; *c*-axis BTO would be preferred so that *r* is consistent in-plane, because $r_{51} = r_{42}$ as induced by crystal symmetry, which would provide more convenience in device design.

Other than the DSO substrate, we have also explored other possible substrates for BTO which have good lattice match and low refractive index. The scandate family, with elements neighboring dysprosium, would have similar lattice parameters and refractive indices. We have thus grown BTO films on several scandate substrates, including $TbScO_3$ (TSO), $GdScO_3$ (GSO), $SmScO_3$ (SSO), $NdScO_3$ (NSO), and managed to achieve high-quality single-crystal BTO films. Additionally, although the lattice mismatch in $La_{0.3}Sr_{0.7}Al_{0.65}Ta_{0.35}O_3$ (LSAT) and $LaSrAlO_4$ (LSAO) would nominally cause strain much larger compared with other substrates tested, these also turned out to be suitable for growth. **Figure 5**a,b show XRD spectra for (≈500 nm-thick) BTO films grown on various substrates in comparison with BTO-on-STO and BTO-on-MgO. The spectra clearly indicate that the films are all *c*-oriented, and the crystal quality is very high as indicated in Figure 5c by the small FWHM of the rocking curve at the BTO (002) Bragg peak.

Other than crystallinity of BTO, we checked other important factors, such as index contrast. Refractive indices of the substrates were measured by spectroscopic ellipsometry, as shown in Figure 5d,e. Compared with indices n_o and n_e of BTO on DSO, the indices of the other substrates tested are all lower.

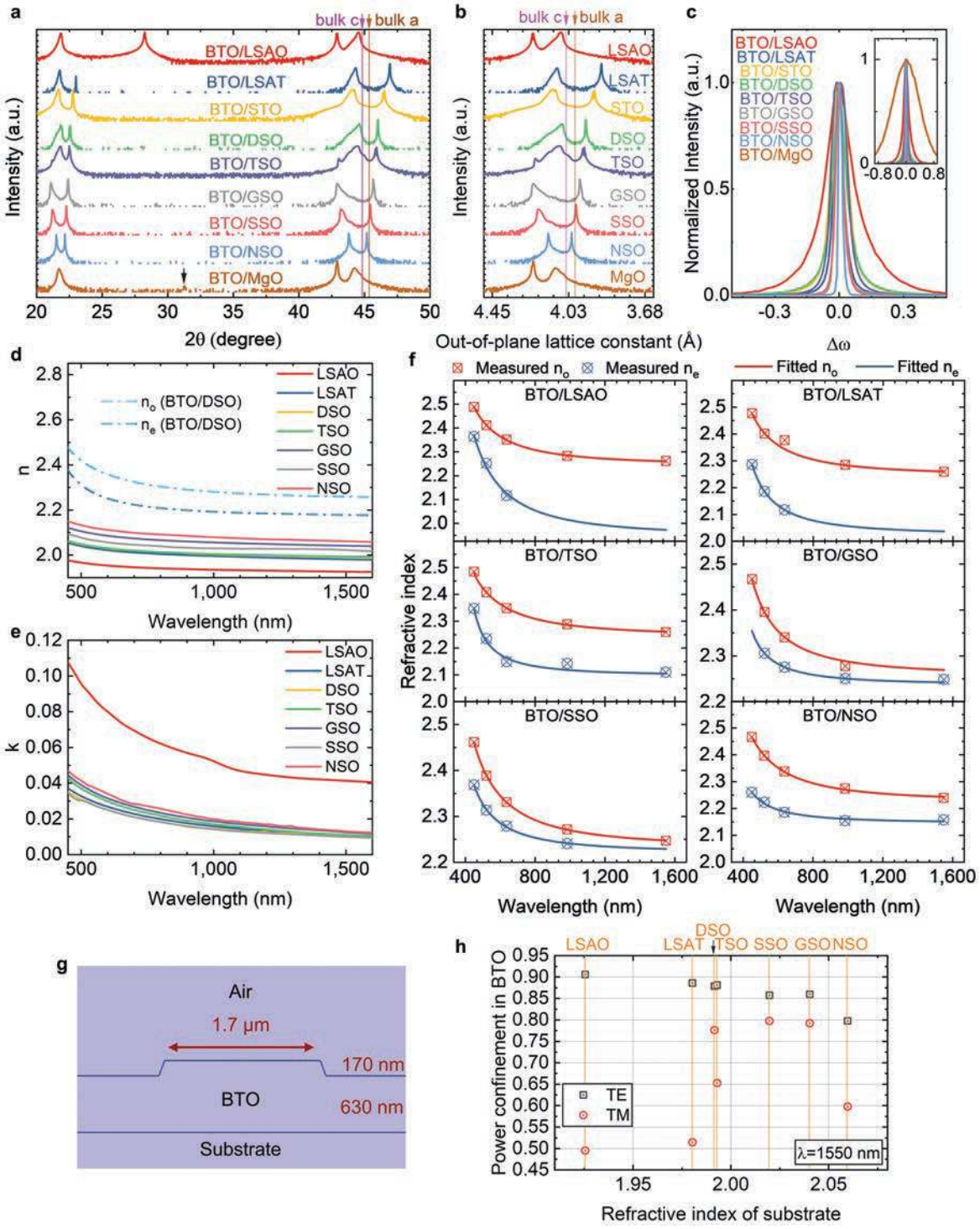

Figure 5. Equivalent substrate alternatives (LSAO, LSAT, DSO, TSO, GSO, SSO, NSO) for the BTO electro-optic platform. a) XRD 2θ–ω coupled scans for BTO films grown on different substrates, all showing single *c*-axis orientation except for BTO on MgO which shows a tiny portion with (110) orientation, indicated by the black arrow. BTO on STO and MgO are plotted for reference. b) Out-of-plane lattice constant converted from (a) near the BTO (002) peak showing a clearer single *c*-axis orientation and different strain states. Note that intensity in (a,b) is on a logarithmic scale. c) Comparison of alignment of crystal orientation along the *z*-axis in the rocking curve at the BTO (002) Bragg peak showing superior crystallinity of BTO films on the proposed substrates compared to MgO. d,e) Real and imaginary refractive indices of the proposed substrates measured by ellipsometry. Refractive indices of BTO film on DSO are plotted as a reference showing that these substrates have lower indices than BTO film. f) Refractive indices of BTO films grown on different substrates as a function of wavelength. n_o, n_e measured at 450, 521, 637, 984, 1308, 1548 nm are fitted with the Sellmeier equation. g,h) Comparison of optical field power confinement in BTO for TE and TM modes for BTO grown on different substrates with an example etched waveguide cross section (as shown schematically in (g)).

To further confirm the optical confinement in BTO thin film grown on these substrates, refractive indices of these samples as shown in Figure 5a,b are measured by the prism coupling method. The results are presented in Figure 5f. Although some of the TM modes did not couple to the waveguide properly, leading to a few spurious index values, the trends are otherwise likely highly accurate. Due to the relaxed nature of the film, the indices do not show a clear trend as a function of strain (Figure S3, Supporting Information).

The indices of BTO and their substrates are utilized to perform cross-sectional mode analysis with a typical waveguide structure (Figure 5g), and optical field confinement within the BTO is evaluated (Figure 5h). The power confinement within BTO (PC_{BTO}) is defined as the optical power distributed in the BTO divided by the total power in the optical mode

$$PC_{BTO} = \frac{\left|\int_{A_{BTO}} Sds\right|}{\left|\int_{A_\infty} Sds\right|} \quad (1)$$

where S is the Poynting vector, and A_{BTO} and A_∞ correspond to the BTO area and mode area, respectively.[26] The results show that all TE modes are well confined, while for TM modes, BTO on LSAO, LSAT, and NSO do not show good confinement. These differences are caused by differing substrate and film indices; for example n_e of BTO-on-TSO is a bit smaller than n_e of BTO-on-DSO while the refractive index of TSO is a bit larger than that of DSO, thus BTO-on-DSO has proportionally more optical power distributed in the BTO layer than in the case of BTO-on-TSO. Therefore, for applications where only the TE mode is used, both platforms are fine, but for applications where the TM mode is used, BTO-on-DSO is a better choice.

3. Conclusion

We have demonstrated high-quality single-crystal thin-film BTO-on-DSO as an alternative optoelectronics platform. We characterized the refractive indices on BTO thin film as functions of wavelength and temperature, and show that such a platform can withstand the high temperatures encountered during fabrication processes. The fabricated BTO-on-DSO waveguides showed a low optical loss of around 2 dB cm^{-1}. We proposed other candidate substrates and explored structural and optical properties of BTO on these substrates. This study provides a rich choice for high quality *c*-axis single-crystal BTO optoelectronics platforms, where easy access to the in plane isotropic properties can be beneficial for the design of photonic and optoelectronic devices. This will be advantageous to multiple fabrication and device application studies to come based on this platform.

4. Experimental Section

Sample Preparation: BTO films were grown by PLD with a KrF laser (248 nm wavelength). Laser energy density is fixed at 1.5 J cm^{-2} and repetition rate is 5 Hz. Deposition was performed at a 650 °C substrate temperature and under 10 mTorr oxygen pressure, followed by post-annealing in an oxygen-rich environment (200 Torr) at 520 °C for 30 min.

Device Fabrication: Optical waveguides were fabricated by electron beam lithography followed by argon-ion milling or inductively coupled plasma (ICP) etching. First a thin layer of Cr was deposited on the BTO thin-film samples, followed by spin coating of photoresist. Then waveguides were patterned by lithography followed by development and subsequently Cr was etched away with Cr etchant. Finally, samples were etched by argon-ion milling or ICP etching (with Ar rather than a standard process gas). End facets of waveguides were first diced and subsequently polished by either focused ion beam (FIB) milling or broad ion beam polishing.

Structural Characterization: XRD was performed in the XDD (X-ray Diffractometry and Development) beamline at Singapore Synchrotron Light Source. The X-ray wavelength was 0.15405 nm. The lattice constants of the BTO thin film were measured from room temperature to 700 °C in reciprocal vector space, with the lattice constant of DSO substrate at room temperature as a reference. Surface topography was characterized by atomic force microscopy (AFM, Park). STEM samples were prepared by a FIB system (FEI Versa 3D) with 30 kV Ga ions, followed by a low-voltage (2 kV) cleaning step. STEM imaging was performed using a JEM-ARM200F (JEOL) microscope equipped with an ASCOR aberration corrector, a cold-field emission gun, and a Gatan Quantum ER spectrometer, operated at 200 kV.

Refractive Indices: Refractive indices of BTO films were measured by the prism coupling method using the Metricon system at the Université Polytechnique Hauts-de-France. During the measurement, TE polarized light was first coupled to obtain n_o and film thickness t, and then TM polarized light was used to calculate n_e with known n_o and t. Refractive indices of substrates were characterized by spectroscopic ellipsometry (J. A. Woollam).

Waveguide Propagation Loss: Propagation loss was measured with both the camera method and the Fabry–Perot method. The laser input and output were directed from a Keysight Lightwave measurement system by optical fiber.

Simulation: Cross-sectional mode analyses were performed by COMSOL Multiphysics.

Acknowledgements

This work was supported by the Singapore National Research Foundation (NRF) under the Competitive Research Programs (CRP Grant No. NRF-CRP15-201501). Y.C, E.D, and A.D. would like to acknowledge Hassan Ahmad for his help in the characterization of optical properties. P.Y. was supported by SSLS via NUS Core Support C-380-003-003-001. The authors would also like to acknowledge the Singapore Synchrotron Light Source (SSLS) for providing the facilities necessary for conducting the research. The SSLS is a National Research Infrastructure under the National Research Foundation Singapore.

[1] R. W. Boyd, *Nonlinear Optics*, 3rd ed., Academic Press, Cambridge, MA, USA **2008**.
[2] A. R. Johnston, J. M. Weingart, *J. Opt. Soc. Am.* **1965**, *55*, 828.
[3] E. D. Palik, *Handbook of Optical Constants of Solids*, Academic Press, USA **1991**.
[4] A. Petraru, J. Schubert, M. Schmid, Ch. Buchal, *Appl. Phys. Lett.* **2002**, *81*, 1375.
[5] P. Tang, D. J. Towner, A. L. Meier, B. W. Wessels, *IEEE Photonics Technol. Lett.* **2004**, *16*, 1837.
[6] P. Tang, D. J. Towner, T. Hamano, A. L. Meier, B. W. Wessels, *Opt. Express* **2004**, *12*, 5962.
[7] B. W. Wessels, *Annu. Rev. Mater. Res.* **2007**, *37*, 659.
[8] D. M. Gill, C. W. Conrad, G. Ford, B. W. Wessels, S. T. Ho, *Appl. Phys. Lett.* **1997**, *71*, 1783.
[9] D. H. Kim, H. S. Kwok, *Appl. Phys. Lett.* **1995**, *67*, 1803.
[10] L. Beckers, J. Schubert, W. Zander, J. Ziesmann, A. Eckau,

P. Leinenbach, Ch. Buchal, *J. Appl. Phys.* **1998**, *83*, 3305.
[11] I.-D. Kim, Y. Avrahami, L. Socci, F. Lopez-Royo, H. L. Tuller, *J. Asian Ceram. Soc.* **2014**, *2*, 231.
[12] F. Leroy, A. Rousseau, S. Payan, E. Dogheche, D. Jenkins, D. Decoster, M. Maglione, *Opt. Lett.* **2013**, *38*, 1037.
[13] A. Petraru, J. Schubert, M. Schmid, O. Trithaveesak, Ch. Buchal, *Opt. Lett.* **2003**, *28*, 2527.
[14] P. Tang, D. J. Towner, A. L. Meier, B. W. Wessels, *Appl. Phys. Lett.* **2004**, *85*, 4615.
[15] C. Wang, M. Zhang, X. Chen, M. Bertrand, A. Shams-Ansari, S. Chandrasekhar, P. Winzer, M. Lončar, *Nature* **2018**, *562*, 101.
[16] E. Dogheche, X. Lansiaux, D. Remiens, *J. Appl. Phys.* **2003**, *93*, 1165.
[17] H. F. Kay, P. Vousden, *Philos. Mag.* **1949**, *40*, 1019.
[18] K. J. Choi, M. Biegalski, Y. L. Li, A. Sharan, J. Schubert, R. Uecker, P. Reiche, Y. B. Chen, X. Q. Pan, V. Gopalan, L.-Q. Chen, D. G. Schlom, C. B. Eom, *Science* **2004**, *306*, 1005.
[19] G. Tittelbach, B. Richter, W. Karthe, *Pure Appl. Opt.* **1993**, *2*, 683.
[20] G. Ulliac, V. Calero, A. Ndao, F. I. Baida, M.-P. Bernal, *Opt. Mater.* **2016**, *53*, 1.
[21] A. Guarino, G. Poberaj, D. Rezzonico, R. Degl'Innocenti, P. Günter, *Nat. Photonics* **2007**, *1*, 407.
[22] P. Rabiei, J. Ma, S. Khan, J. Chiles, S. Fathpour, *Opt. Express* **2013**, *21*, 25573.
[23] H. Hu, R. Ricken, W. Sohler, *Opt. Express* **2009**, *17*, 24261.
[24] M. F. Volk, S. Suntsov, C. E. Rüter, D. Kip, *Opt. Express* **2016**, *24*, 1386.
[25] S. Abel, F. Eltes, J. E. Ortmann, A. Messner, P. Castera, T. Wagner, D. Urbonas, A. Rosa, A. M. Gutierrez, D. Tulli, P. Ma, B. Baeuerle, A. Josten, W. Heni, D. Caimi, L. Czornomaz, A. A. Demkov, J. Leuthold, P. Sanchis, J. Fompeyrine, *Nat. Mater.* **2019**, *18*, 42.
[26] P. Berini, *Phys. Rev. B* **2000**, *61*, 10484.